Clean-to-Composite Bound Ratio: A Multipath Criterion for GNSS Signal Design and Analysis

Corentin Lubeigt, Lorenzo Ortega, Jordi Vilà-Valls, *Senior Member, IEEE*, Laurent Lestarquit, Eric Chaumette, *Member, IEEE*

***Abstract*—Multipath is one of the most challenging propagation conditions affecting Global Navigation Satellite Systems (GNSS), which must be mitigated in order to obtain reliable navigation information. In any case, the random multipath nature makes it difficult to anticipate and overcome. Therefore, for legacy GNSS signal performance assessment, modern GNSS signal design and future GNSS-based applications, robustness to multipath is a fundamental criterion. Different multipath metrics exist in the literature, such as the multipath error envelope, usually leading to analyses only valid for a dedicated receiver/signal combination and only providing information on the bias. This paper presents a general criterion to characterize the multipath robustness of a generic band-limited signal (e.g., GNSS or radar), considering the joint delay-Doppler and phase estimation. This criterion is based on the Cramér-Rao bound, which makes it universal, regardless the receiver architecture and the signal under analysis, and provides information on the actual achievable performance in terms of estimated time-delay (i.e., pseudo-range) and Doppler frequency variances.**

***Index Terms*—GNSS, multipath, delay/Doppler and phase estimation, Cramér-Rao bound, signal analysis, maximum likelihood estimation.**

I. Introduction

THE use of Global Navigation Satellite Systems (GNSS) signals spans over a plethora of applications, from its original navigation purposes [1], [2], to precise time synchronization, remote sensing of the ionosphere for earthquake forecasting, reflectometry (GNSS-R) [3] or radio occultation, to name a few. Therefore, there exists a clear interest to have meaningful tools for the correct characterization of legacy GNSS signals, but also for the design of new signals for these purposes or modern applications to come. There are different signal design and analysis performance criteria depending on the final application at hand, e.g., positioning accuracy, anti-jamming capabilities, fast signal re-acquisition or resilience to multipath. The latter still remains an open issue impacting several applications, indeed being the limiting factor in several scenarios due to the environment specific nature of such harsh propagation conditions. For instance, i) multipath is one of the main propagation challenges impairing navigation capabilities in urban environments, ii) diffuse multipath is a fundamental problem in near indoor conditions, which is a challenge for precise time synchronization at the core of next generation 5G small cells, or iii) it may have a clear impact in ground-based or low altitude airborne GNSS-R [4], [5], where depending on the system geometry the direct signal may leak into the antenna dedicated to the reflected signal [6], [7], directly degrading the final GNSS-R product. In any case, to assess the impact of possible multipath conditions into the final system performance, accurate metrics are required.

From previous GNSS signal design contributions [8]–[11] it is clear that the de facto metric used to characterize multipath is the so-called multipath error envelope (MPEE) [12]–[14]. The MPEE estimates the multipath-induced error, considering a simple two-ray model and a specific receiver architecture, as a function of the geometrical propagation delay. It is evaluated by taking the bias on the line-of-sight (LOS) signal delay of a given estimator in a noise-free environment.

This metric has been widely applied to any multipath mitigation method that were developed ever since. These methods can be divided into two main categories: i) correlator-based algorithms such as Pulse Aperture Correlator (PAC) [15], Vision Correlator (VC) [16] or High Resolution Correlator (HRC) [17] where the idea is to account for the multipath by adding a small number of correlators and by evaluating how the multipath distorts the correlation function; and ii) more sophisticated algorithms that are estimating the parameters of the multipath such as the Multipath Mitigation Technique (MMT) [18], the Multipath Estimating Delay Lock Loop (MEDLL) [19], [20], Space-Alternating Generalized Expectation-Maximization (SAGE) [21] or, more recently, the enhanced Coupled Amplitude Delay Lock Loops (CADLL) [22], [23]. With MPEE it is then possible to compare these algorithms with each other and with different GNSS signals such as in [24], [25] where the size of the MPEE and the moment it reduces to zero when the path separation gets larger tell the potential user how well the studied algorithm performs.

In this work, a fundamentally different and more general approach to multipath error characterization is proposed. A metric to evaluate the robustness to multipath of any band-limited signal candidate (e.g., GNSS or radar signals) is derived by resorting to the Cramér-Rao bound (CRB). Indeed, the ratio between the single source delay-Doppler CRB [26] and the corresponding dual source delay-Doppler CRB [27], considering a generic band-limited signal, provides the exact loss in delay and Doppler estimation capabilities, which in turn naturally translates to the final position estimates. One of the key advantages of this closed-form metric is that it

C. Lubeigt is with University of Toulouse TéSA/ISAE-Supaero, 31500, Toulouse, France, e-mail: corentin.lubeigt@tesa.prd.fr; L. Ortega is with IPSA, 31000, Toulouse, France, e-mail: lorenzo.ortega@ipsa.fr; J. Vilà-Valls and E. Chaumette are with University of Toulouse, ISAE-Supaero, 31400, Toulouse, France, e-mail: {jordi.vila-valls, eric.chaumette}@isae-supaero.fr; L. Lestarquit is with CNES, 31400, Toulouse, France, e-mail: laurent.lestarquit@cnes.fr; This research was partially supported by the CNES and the DGA/AID projects (2019.65.0068.00.470.75.01, 2021.65.0070.00.470.75.01).

only depends on the baseband signal samples, and therefore does not require to assume any specific receiver architecture, thus providing a general multipath error performance limit. Additional advantages can be listed as follows, this ratio is valid for any signal-to-noise ratio (SNR) level and does not depend on the amplitude of the multipath, as it is shown in the derivation of the closed-form. Representative GNSS signals are compared in terms of the proposed metric to support the discussion.

The article is organized as follows: Section II presents the existing MPEE, a simple alternative and their limits. Section III provides the theoretical background needed for the metric, which is derived in Section IV. Section V presents representative results and the corresponding discussion. A conclusion on this work is drawn in Section VI.

II. Multipath Error Envelope

The effect of multipath on the receiver performance is a complex problem that has been addressed from several perspectives [12], [28]. The first criterion to deal with multipath is the multipath model itself. A simple approach, widely used for signal design, is the specular multipath model that assumes a single multipath impinging on the receiver antenna and distorting the line-of-sight (LOS) signal of interest. This model considers a single specular reflection of the LOS signal. For a given multipath-to-direct ratio (MDR), one can study the impact of the non-line-of-sight (NLOS) signal on the LOS signal delay estimation. This study usually does not take into account the noise (i.e., SNR tends towards infinity). A typical output of the specular multipath model is the so-called MPEE that represents the worst case impact of the NLOS over the LOS signal. These worst cases are obtained when the NLOS is in-phase (relative phase $\Delta\phi = 0$) and out-of-phase ($\Delta\phi = \pi$). It is defined as follows [12, (9.65)]:

$$\left(\max_{\Delta\phi}\left(e\left(\rho_1/\rho_0, \Delta\tau, \Delta\phi\right)\right), \min_{\Delta\phi}\left(e\left(\rho_1/\rho_0, \Delta\tau, \Delta\phi\right)\right)\right) \tag{1}$$

where $e(\cdot)$ is the induced bias on the estimation of the LOS delay, ρ_1/ρ_0 is the MDR, $\Delta\tau$ is the excess delay of the multipath with respect to (w.r.t.) the LOS. Even though such a model is not realistic, it quickly provides an idea of an estimator behavior for a given signal in presence of multipath, and is widely used [13], [14], [24]. The MPEE output is the error (in meters) on the LOS pseudo-range estimation induced by the NLOS w.r.t. a given excess delay, often converted into path separation. From a statistical point of view, MPEE can be seen as the bias envelope of the misspecified estimator considered. Fig. 1 and Fig. 2 show the MPEE for GPS L1 C/A and Galileo E1B signals with the MMT estimator, which is an implementation of the dual source maximum likelihood estimator (MLE) [18] and the MEDLL estimator [19], [20] which is also known as CLEAN-RELAX estimator.

From these two figures, one can first note that for the MMT estimator, the MPEE is a flat zero-valued line. Indeed, when there is no noise, the dual source maximum likelihood estimator (2S-MLE) is unbiased and, consequently, MPEE will not provide any information. Concerning the MEDLL, one can see that the MPEE reaches zero for path separation greater than

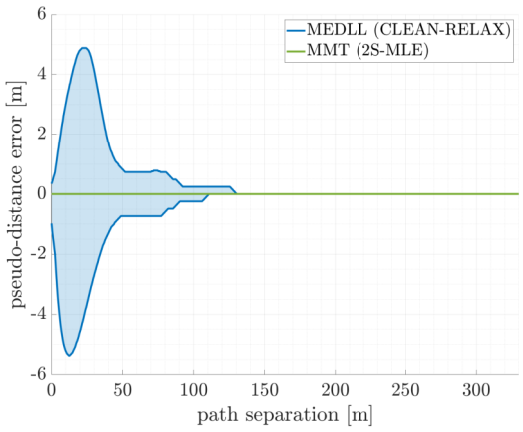

Fig. 1. MPEE applied to MEDLL and MMT estimators for GPS L1 C/A signal. Front-end filter bandwidth set to 12 MHz, MDR = 0.5, integration time T_I = 1ms.

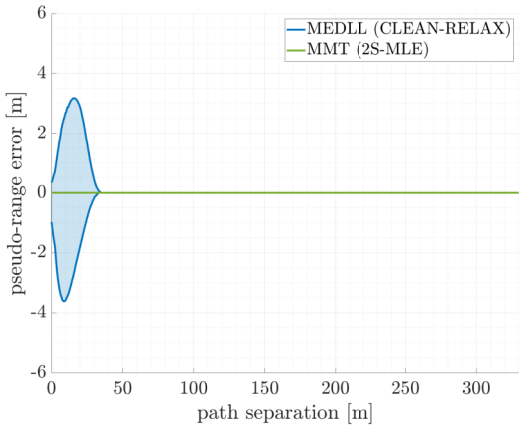

Fig. 2. MPEE applied to MEDLL and MMT estimators for Galileo E1B signal. Front-end filter bandwidth set to 12 MHz, MDR = 0.5, integration time T_I = 4ms.

140m for GPS L1 C/A and 40m for Galileo E1B. After these values, the estimator can be said unbiased, but there is no way to say whether its variance in a noisy environment will reach a lower bound or not.

An alternative to the often too simplistic MPEE can be obtained using the Root Mean Square error (RMSE) output of a considered estimator as it is used in [29]. The multipath impact with a random relative phase uniformly distributed in $(0, 2\pi)$ is studied in [18], where the result is linked to the CRB reached by either a MLE or minimum mean square error (MMSE) estimator [30]. In this case, the noise is taken into account by setting a SNR. In Fig. 3 and Fig. 4, the RMSE for the estimation of the LOS delay is plotted as a function of the path separation. These figures were obtained with 1000 Monte Carlo simulations, when the LOS and the multipath are in-phase. The SNR, defined at the output of the matched filter is defined as follows

$$\mathrm{SNR}_{\mathrm{out}} = \frac{\rho_0^2 \mathbf{s}^H \mathbf{s}}{\sigma_n^2} = (C/N_0)\, T_I \tag{2}$$

where ρ_0 is the amplitude of the LOS signal, σ_n^2 is the

variance of an additive white gaussian noise, the baseband signal samples are

$$\mathbf{s} = \left(\quad \dots \quad s(nT_s) \quad \dots \quad \right)^T_{N_1 \le n \le N_2}, \tag{3}$$

C/N_0 is the carrier-to-noise power density ratio and T_I is the coherent integration time, T_s being the sampling period.

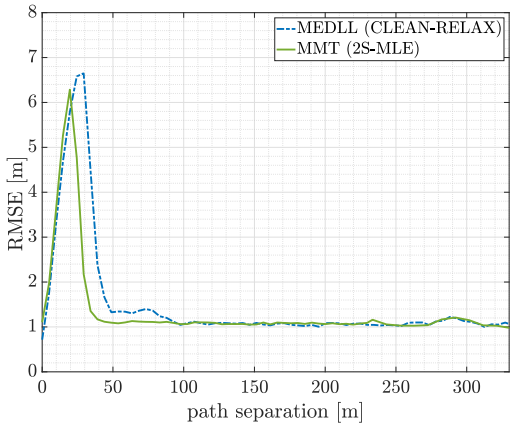

Fig. 3. RMSE of the MEDLL and MMT estimators for GPS L1 C/A signal. Front-end filter bandwidth set to 12 MHz, MDR = 0.5, integration time T_I = 1ms, SNR_{out} = 31dB.

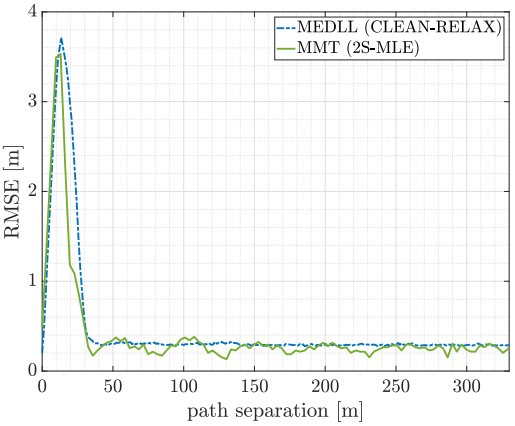

Fig. 4. RMSE of the MEDLL and MMT estimators for Galileo E1B signal. Front-end filter bandwidth set to 12 MHz, MDR = 0.5, integration time T_I = 4ms, SNR_{out} = 34dB.

Even though one can find similarities between the MPEE and the RMSE, they are very different: the former provides information on the bias of an estimator and the latter provides information on the bias and the variance. Besides, the RMSE adds extra information: for instance, in Fig. 3, the RMSE of both MMT and MEDLL seem lower bounded at 1m and present a variation at around 300m, which corresponds to 1 C/A chip. That bound is reached at 40m for the MMT and 100 for the MEDLL. In Fig. 4, there is also a lower bound at about 30cm of RMSE and both MMT and MEDLL reach it at a path separation of 40m. Since these bounds are reached when the estimators are unbiased, they might be related to the CRB that characterize efficient estimators.

These two last figures present a strong interest as they provide information where the MPEE does not. However they lack of generality: the noise level must be fixed, several of Monte Carlo simulations need to be run for each point and one cannot easily tell how this RMSE varies when the relative phase and the relative amplitude vary.

In short, MPEE is characterizing the bias induced by a multipath to an estimator/signal set. It is useful a tool to compare different receiver architectures for the same signal, or different signals for the same architecture, but does not provide information anymore when the estimator is unbiased. The RMSE approach in [18] is fundamentally different: using an unbiased estimator, like the MLE in the asymptotic region (i.e., at high SNR where it is efficient [31]), the multipath impact is linked to the global achievable estimation accuracy. This does not depend on the architecture anymore and only relies on the signal structure, but as it is based on the performance of a specific estimator, the results can only be obtained after exhaustive Monte Carlo analysis. If one looks at the following definition

$$(\text{RMSE})^2 = \underbrace{\text{variance}}_{\text{CRB}} + \underbrace{(\text{bias})^2}_{\text{MPEE}}, \tag{4}$$

it is then clear that a relevant complementary tool to MPEE is necessarily based on the CRB.

In this article, a generalized approach based on the delay-Doppler CRB is proposed. Where widely used MPEE, based on a sub-optimal single source criterion, studies the intrinsic limits of a given architecture, only providing information on the bias, the CRB approach, based on a dual source criterion aims at studying the intrinsic limits of a given signal. Exploiting these bounds provides a meaningful way to complete and simplify the work in [18] because it does not depend on a specific estimator and provides a general multipath error performance.

III. Signal Model and Insights on the CRB

A. Signal Model

Let a transmitter T and a receiver R have uniform linear motions such that the positions can be described as $\mathbf{p}_T(t) = \mathbf{p}_T + \mathbf{v}_T t$ and $\mathbf{p}_R(t) = \mathbf{p}_R + \mathbf{v}_R t$, where $\mathbf{p}$ and $\mathbf{v}$ are the position and velocity vectors, respectively. Under such conditions, the distance between T and R at instant t can be approximated by a first order distance-velocity model:

$$\begin{aligned} &\|\mathbf{p}_{TR}(t)\| \triangleq \|\mathbf{p}_R(t) - \mathbf{p}_T(t - \tilde{\tau}(t))\| = c\tilde{\tau}(t) \approx d + vt, \\ &\tilde{\tau}(t) \approx \tau + bt, \ \ \tau = \frac{d}{c}, \ \ b = \frac{v}{c}, \end{aligned} \tag{5}$$

where d is the T-to-R absolute distance when $t = 0$, v is the T-to-R radial velocity, τ is the time-delay due to the propagation path, $(1-b)$ is the dilatation induced by the Doppler effect, and c is the speed of light in a vacuum. A band-limited signal $s(t)$, with bandwidth B, is transmitted by T over a carrier frequency f_c ($\lambda_c = c/f_c$). Notice that this signal model encompasses any GNSS signal. Using (5), the dual source complex analytic signal at the output of the receiver's antenna is:

$$x_R(t) = d_R(t;\boldsymbol{\eta}_0,\rho_0,\phi_{R,0}) + d_R(t;\boldsymbol{\eta}_1,\rho_1,\phi_{R,1}) + w_R(t), \quad (6)$$

$$d_R(t;\boldsymbol{\eta}_i,\rho_i,\phi_{R,i}) = \rho_i e^{j\phi_{R,i}} s((1-b_i)(t-\tau_i)) e^{j\omega_c(1-b_i)t} e^{-j\omega_c\tau_i}, \quad (7)$$

where $w_R(t)$ is a zero-mean white complex circular Gaussian noise, $\omega_c = 2\pi f_c$, and for $i \in \{0,1\}$, $\boldsymbol{\eta}_i^T = [\tau_i, b_i]$, and ρ_i and $\phi_{R,i}$ are the amplitude (real number strictly positive) and phase of the complex coefficients induced by the propagation characteristics (fading, reflection, *etc.*), the polarization mismatches and the antenna gains. In this study, since a single specular reflection is considered, signal 0 will refer to the LOS signal where signal 1 will refer to the single multipath, also noted NLOS. Under the narrowband signal hypothesis, the Doppler effect on the band-limited baseband signal $s(t)$ is usually neglected so that: $s((1-b)(t-\tau)) \approx s(t-\tau)$ [32, Ch.9]. Therefore, the baseband output of the receiver's Hilbert filter containing a direct signal and a single specular reflection can be approximated by

$$x(t) \triangleq x_R(t)e^{-j\omega_c t} = d(t;\boldsymbol{\theta}_0) + d(t;\boldsymbol{\theta}_1) + w(t)\ , \quad (8)$$

$$d(t;\boldsymbol{\theta}_i) \triangleq \rho_i e^{j\phi_i} a(t;\boldsymbol{\eta_i})\ , \quad (9)$$

$$a(t;\boldsymbol{\eta_i}) \triangleq s(t-\tau_i)e^{-j\omega_c b_i(t-\tau_i)}\ , \quad (10)$$

where for $i \in \{0,1\}$, $\boldsymbol{\theta}_i^T = [\boldsymbol{\eta}_i^T, \rho_i, \phi_i]$, $\phi_i = \phi_{R,i} - \omega_c(1+b_i)\tau_i$. If we now consider the acquisition of $N = N_2 - N_1 + 1$ samples at a sampling frequency $F_s = 1/T_s$, set equal to the front-end bandwidth of the receiver B_R, the discrete signal model yields to the following dual source conditional signal model (CSM),

$$\mathbf{x} = \mathbf{A}(\boldsymbol{\eta}_0,\boldsymbol{\eta}_1)\boldsymbol{\alpha} + \mathbf{w},\ \mathbf{w} \sim \mathcal{CN}(0,\sigma_n^2\mathbf{I}_N)\ , \quad (11)$$

with, for $n \in [N_1, N_2]$,

$$\begin{aligned}
&\mathbf{x}^T = (\ldots,\ x(nT_s),\ \ldots)\ ,\\
&\mathbf{A}(\boldsymbol{\eta}_0,\boldsymbol{\eta}_1) = \left[\mathbf{a}(\boldsymbol{\eta}_0),\ \mathbf{a}(\boldsymbol{\eta}_1)\right]\ ,\\
&\mathbf{a}^T(\boldsymbol{\eta}_i) = \left(\ldots,\ s(nT_s-\tau_i)e^{-j\omega_c b_i(nT_s-\tau_i)},\ \ldots\right)\ ,\\
&\boldsymbol{\alpha}^T = \left(\rho_0 e^{j\phi_0},\ \rho_1 e^{j\phi_1}\right)\ ,\\
&\mathbf{w}^T = (\ldots,\ w(nT_s),\ \ldots)\ .
\end{aligned}$$

B. Insights and Extension of the CRB for the Reception of a Delayed, Dilated and Reflected Signal

The parameters to be estimated are gathered in the following vector: $\boldsymbol{\epsilon}^T = [\sigma_n^2, \boldsymbol{\eta}_0^T, \boldsymbol{\eta}_1^T, \rho_0, \phi_0, \rho_1, \phi_1]$. From (11), one can write $\mathbf{x} \sim \mathcal{CN}\left(\mathbf{A}(\boldsymbol{\eta}_0,\boldsymbol{\eta}_1)\boldsymbol{\alpha}, \sigma_n^2\mathbf{I}_N\right)$ and the probability density function (pdf) is expressed as,

$$p(\mathbf{x},\boldsymbol{\epsilon}) = \frac{1}{\left(\pi\sigma_n^2\right)^N} e^{-\frac{1}{\sigma_n^2}\|\mathbf{x}-\mathbf{A}(\boldsymbol{\eta}_0,\boldsymbol{\eta}_1)\boldsymbol{\alpha}\|^2}\ . \quad (12)$$

The corresponding CRB for the estimation of $\boldsymbol{\epsilon}$ is defined as the inverse of the Fisher Information Matrix (FIM) [33],

$$\mathbf{CRB}_{\boldsymbol{\epsilon}|\boldsymbol{\epsilon}} = \mathbf{F}_{\boldsymbol{\epsilon}|\boldsymbol{\epsilon}}^{-1}(\boldsymbol{\epsilon}),\ \mathbf{F}_{\boldsymbol{\epsilon}|\boldsymbol{\epsilon}}(\boldsymbol{\epsilon}) = -E\left[\frac{\partial^2 \ln p(\mathbf{x},\boldsymbol{\epsilon})}{\partial\boldsymbol{\epsilon}\partial\boldsymbol{\epsilon}^T}\right]\ . \quad (13)$$

From [34, (4.68)], one can find the expression of the CRB for the estimation of the parameters of interest gathered in the concatenated vector $\overline{\boldsymbol{\eta}}_2^T = [\boldsymbol{\eta}_0^T, \boldsymbol{\eta}_1^T]$ based on a single observation of the signal:

$$\mathbf{CRB}_{\overline{\boldsymbol{\eta}}_2|\boldsymbol{\epsilon}}^{-1}(\boldsymbol{\epsilon}) = \frac{2}{\sigma_n^2}\mathrm{Re}\left\{\boldsymbol{\Phi}\left(\overline{\boldsymbol{\eta}}_2\right) \odot \left(\mathbf{R}_{\boldsymbol{\alpha}}^T \otimes \begin{bmatrix} 1 & 1 \\ 1 & 1 \end{bmatrix}\right)\right\}, \quad (14)$$

$$\mathbf{R}_{\boldsymbol{\alpha}} = \boldsymbol{\alpha}\boldsymbol{\alpha}^H = \begin{bmatrix} \rho_0^2 & \rho_0\rho_1 e^{-j(\phi_1-\phi_0)} \\ \rho_0\rho_1 e^{j(\phi_1-\phi_0)} & \rho_1^2 \end{bmatrix}, \quad (15)$$

$$\boldsymbol{\Phi}\left(\overline{\boldsymbol{\eta}}_2\right) = \begin{bmatrix} \frac{\partial \mathbf{a}^H(\boldsymbol{\eta}_0)}{\partial\boldsymbol{\eta}_0} \\ \frac{\partial \mathbf{a}^H(\boldsymbol{\eta}_1)}{\partial\boldsymbol{\eta}_1} \end{bmatrix} \mathbf{P}^{\perp}_{\mathbf{A}(\overline{\boldsymbol{\eta}}_2)} \begin{bmatrix} \frac{\partial \mathbf{a}^H(\boldsymbol{\eta}_0)}{\partial\boldsymbol{\eta}_0} \\ \frac{\partial \mathbf{a}^H(\boldsymbol{\eta}_1)}{\partial\boldsymbol{\eta}_1} \end{bmatrix}^H, \quad (16)$$

where $\mathbf{P}_{\mathbf{A}} = \mathbf{I} - \mathbf{P}^{\perp}_{\mathbf{A}} = \mathbf{A}\left(\mathbf{A}^H\mathbf{A}\right)^{-1}\mathbf{A}^H$ is the orthogonal projector onto the subspace defined by the set of the column vectors of matrix $\mathbf{A}$, $\odot$ denotes the Hadamard product and $\otimes$ denotes the Kronecker product.

If one notes $\Gamma = |\Gamma|e^{j\phi_\Gamma}$ such that $\rho_1 e^{j\phi_1} = \Gamma\rho_0 e^{j\phi_0}$, the CRB defined in (14) can be further developed and written as:

$$\mathbf{CRB}_{\overline{\boldsymbol{\eta}}_2|\boldsymbol{\epsilon}}^{-1}(\boldsymbol{\epsilon}) = \frac{2\rho_0^2}{\sigma_n^2}\mathrm{Re}\left\{\begin{bmatrix} \boldsymbol{\Phi}_{1,1} & \Gamma^*\boldsymbol{\Phi}_{2,1}^H \\ \Gamma\boldsymbol{\Phi}_{2,1} & |\Gamma|^2\boldsymbol{\Phi}_{2,2} \end{bmatrix}\right\}. \quad (17)$$

Proof. see Appendix A for details on the derivation of submatrices $\boldsymbol{\Phi}_{i,j}$, $i,j = \{1,2\}$. □

Then, using the block matrix inversion lemma (53) on (17), the inverse of $\mathbf{CRB}_{\boldsymbol{\eta}_0|\boldsymbol{\epsilon}}$ can be expressed as

$$\mathbf{CRB}_{\boldsymbol{\eta}_0|\boldsymbol{\epsilon}}^{-1}(\boldsymbol{\epsilon}) = \frac{2\rho_0^2}{\sigma_n^2}\left(\mathbf{A}_\Phi - \mathbf{B}_\Phi - \cos(2\phi_\Gamma)\mathbf{C}_\Phi + \sin(2\phi_\Gamma)\mathbf{D}_\Phi\right), \quad (18)$$

where, with superscript R and I standing for real and imaginary parts, respectively,

$$\mathbf{A}_\Phi = \boldsymbol{\Phi}_{1,1}^R, \quad (19)$$

$$\mathbf{B}_\Phi = \frac{1}{2}\left(\boldsymbol{\Phi}_{2,1}^R\left(\boldsymbol{\Phi}_{2,2}^R\right)^{-1}\boldsymbol{\Phi}_{2,1}^R + \boldsymbol{\Phi}_{2,1}^I\left(\boldsymbol{\Phi}_{2,2}^R\right)^{-1}\boldsymbol{\Phi}_{2,1}^I\right), \quad (20)$$

$$\mathbf{C}_\Phi = \frac{1}{2}\left(\boldsymbol{\Phi}_{2,1}^R\left(\boldsymbol{\Phi}_{2,2}^R\right)^{-1}\boldsymbol{\Phi}_{2,1}^R - \boldsymbol{\Phi}_{2,1}^I\left(\boldsymbol{\Phi}_{2,2}^R\right)^{-1}\boldsymbol{\Phi}_{2,1}^I\right), \quad (21)$$

$$\mathbf{D}_\Phi = \frac{1}{2}\left(\boldsymbol{\Phi}_{2,1}^R\left(\boldsymbol{\Phi}_{2,2}^R\right)^{-1}\boldsymbol{\Phi}_{2,1}^I + \boldsymbol{\Phi}_{2,1}^I\left(\boldsymbol{\Phi}_{2,2}^R\right)^{-1}\boldsymbol{\Phi}_{2,1}^R\right). \quad (22)$$

Proof. see Appendix B. □

Note that in (18), the CRB does not depend on $|\Gamma|$. This means that in the asymptotic region of operation of the 2S-MLE, the estimation of both the time delay and the Doppler frequency of the LOS signal is not affected by the relative amplitude of the NLOS but only by its relative delay, Doppler and phase.

Equation (18) being a two-by-two matrix, it is easy to evaluate its inverse and then extract a closed-form of $\mathrm{CRB}_{\tau_0|\boldsymbol{\epsilon}}$:

$$\mathrm{CRB}_{\tau_0|\boldsymbol{\epsilon}}(\boldsymbol{\epsilon}) = \frac{\sigma_n^2}{2\rho_0^2}\frac{\left[\mathbf{A}_\Phi - \mathbf{B}_\Phi - \cos(2\phi_\Gamma)\mathbf{C}_\Phi + \sin(2\phi_\Gamma)\mathbf{D}_\Phi\right]_{2,2}}{\det\left(\mathbf{A}_\Phi - \mathbf{B}_\Phi - \cos(2\phi_\Gamma)\mathbf{C}_\Phi + \sin(2\phi_\Gamma)\mathbf{D}_\Phi\right)} \quad (23)$$

where $\det(\cdot)$ is the determinant of the matrix in argument. Similarly, a closed-form expression of the CRB for the estima-

tion of the LOS Doppler parameter b_0 can be easily obtained by taking the other diagonal term of the inverse matrix:

$$\begin{aligned}&\mathrm{CRB}_{b_0|\boldsymbol{\epsilon}}(\boldsymbol{\epsilon})\\&=\frac{\sigma_n^2}{2\rho_0^2}\frac{[\mathbf{A}_\Phi-\mathbf{B}_\Phi-\cos(2\phi_\Gamma)\mathbf{C}_\Phi+\sin(2\phi_\Gamma)\mathbf{D}_\Phi]_{1,1}}{\det\left(\mathbf{A}_\Phi-\mathbf{B}_\Phi-\cos(2\phi_\Gamma)\mathbf{C}_\Phi+\sin(2\phi_\Gamma)\mathbf{D}_\Phi\right)}\end{aligned}\tag{24}$$

As a side note, the derived CRB presented in (23) and (24) are just alternative formulations of the CRB that were already derived in [27].

IV. A Criterion Based on Cramér-Rao Bounds: Clean-to-Composite Bound Ratio

A. Definition for the time-delay

The case without signal reflection is equivalent to a well known standard single source scenario. The corresponding closed-form CRB was derived in [26]. The resulting CRBs are recalled here:

$$\mathrm{CRB}_{\tau_0|\boldsymbol{\theta}_0,\sigma_n^2}=\frac{\sigma_n^2}{2\rho_0^2}\left[\mathbf{A}^{-1}_{\Phi|\boldsymbol{\eta}_1=\mathbf{0}}\right]_{1,1}.\tag{25}$$

where $\mathbf{A}_{\Phi|\boldsymbol{\eta}_1=\mathbf{0}}$ is the matrix $\mathbf{A}_\Phi$ defined in (19) where all the NLOS components are set to zero: $\boldsymbol{\eta}_1=\mathbf{0}$. This way the interference terms are eliminated and the result is exactly the closed-form bound from [26, (17a)].

Then, by simply dividing the CRB in a single source context (25) by the corresponding CRB in a dual source source context (23), a generalized closed-form formulation of a Clean-to-Composite Bound Ratio (CCBR) for the time-delay estimation is obtained, which is expressed with the baseband signal samples (i.e., valid for any band-limited signal):

$$\begin{aligned}\mathrm{CCBR}_\tau(\Delta\tau,b_0,b_1,\phi_\Gamma)&\triangleq\frac{\mathrm{CRB}_{\tau_0|\boldsymbol{\theta}_0,\sigma_n^2}}{\mathrm{CRB}_{\tau_0|\boldsymbol{\epsilon}}}\\&=\frac{\left[\mathbf{A}_{\boldsymbol{\Phi}}^{-1}\right]_{1,1}\det\left(\mathbf{A}_\Phi-\mathbf{B}_\Phi-\cos(2\phi_\Gamma)\mathbf{C}_\Phi+\sin(2\phi_\Gamma)\mathbf{D}_\Phi\right)}{[\mathbf{A}_\Phi-\mathbf{B}_\Phi-\cos(2\phi_\Gamma)\mathbf{C}_\Phi+\sin(2\phi_\Gamma)\mathbf{D}_\Phi]_{2,2}}\end{aligned}\tag{26}$$

where the dependency on $\Delta\tau=\tau_1-\tau_0$ was shown in [27].

First, notice that the CCBR_τ does not depend on the SNR of the LOS and the NLOS. Besides, as previously noticed, this ratio does not depend on the relative amplitude of the reflected signal either but it depends on the relative phase between the LOS and the NLOS signals. Actually, the CCBR_τ is π-periodic w.r.t. ϕ_Γ which reduces its study to the interval $(0,\pi)$ as shown in the next section.

B. Statistics of the Clean-to-Composite Bound Ratio

The π-periodicity of the CCBR_τ can be used to easily obtain the maximum and minimum values for each scenario defined by the set of parameters of interest $(\Delta\tau,b_0,b_1)$. Indeed, by implementing the different matrices required to compute this ratio, it is quite direct to obtain these values. If one sets a pdf to the relative phase ϕ_Γ, it is then also possible to obtain an average value of the CCBR_τ. For instance, one can assume the relative phase to be a random variable uniformly distributed over $(0,\pi)$, then the average can be numerically obtained as:

$$E_{\phi_\Gamma}\left\{\mathrm{CCBR}_\tau\right\}(\Delta\tau,b_0,b_1)=\frac{1}{\pi}\int_0^\pi\mathrm{CCBR}_\tau(\Delta\tau,b_0,b_1,\phi)\mathrm{d}\phi\tag{27}$$

C. Definition for the Doppler frequency

Similarly, it is possible to construct a CCBR_b that can be defined as the ratio between the CRB for the estimation of the LOS Doppler parameter b_0 in a single source context,

$$\mathrm{CRB}_{b_0|\boldsymbol{\theta}_0,\sigma_n^2}=\frac{\sigma_n^2}{2\rho_0^2}\left[\mathbf{A}^{-1}_{\Phi|\boldsymbol{\eta}_1=\mathbf{0}}\right]_{2,2},\tag{28}$$

and the corresponding CRB in a dual source context (24):

$$\begin{aligned}\mathrm{CCBR}_b(\Delta\tau,b_0,b_1,\phi_\Gamma)&\triangleq\frac{\mathrm{CRB}_{b_0|\boldsymbol{\theta}_0,\sigma_n^2}}{\mathrm{CRB}_{b_0|\boldsymbol{\epsilon}}}\\&=\frac{\left[\mathbf{A}_{\boldsymbol{\Phi}}^{-1}\right]_{2,2}\det\left(\mathbf{A}_\Phi-\mathbf{B}_\Phi-\cos(2\phi_\Gamma)\mathbf{C}_\Phi+\sin(2\phi_\Gamma)\mathbf{D}_\Phi\right)}{[\mathbf{A}_\Phi-\mathbf{B}_\Phi-\cos(2\phi_\Gamma)\mathbf{C}_\Phi+\sin(2\phi_\Gamma)\mathbf{D}_\Phi]_{1,1}}\end{aligned}\tag{29}$$

Again, this CCBR does not depend on the SNR nor the relative amplitude. It is also π-periodic w.r.t. ϕ_Γ.

V. Results and Discussions

A. Averaged $CCBR_\tau$

The resulting CCBR_τ with respect to the path separation starts from 0 when the LOS and NLOS signals are perfectly superimposed, in this case both sources are extremely hard to separate and estimating them both properly would imply a very large variance. Then the CCBR_τ tends towards unity when the path separation gets large, and it may present local minima in its transition region. Considering a GPS L1 C/A signal, averaged CCBR_τ results are presented in Fig. 5 for different receivers' RF front-ends. As defined in Section III, the sampling frequency is assumed equal to the front-end bandwidth: $B_R=1$ MHz denotes then a low cost receiver and $B_R=8$ MHz corresponds to higher quality one. In this figure, the relative phase is assumed uniformly distributed in $(0,\pi)$ and, the Doppler frequencies of both signals are arbitrarily set to 0 Hz to obtain the following figures. One can see the effect of the RF front-end bandwidth B_R: when it gets larger, the main signal is less affected by the multipath. It is interesting to see how the averaged CCBR_τ oscillates when the path separation is below 300 meters (i.e., 1 L1 C/A chip), especially for $B_R=8$ MHz, where a peak at about 300 meters suggests a strong sensitivity to multipath of the C/A code for this specific path separation. In other words, for Binary Phase Shift Keying (BPSK(1)) modulations, the LOS signal time-delay estimation is particularly affected when the reflected signal appears at around 1 L1 C/A chip. A discussion regarding this behaviour is proposed in Section V-E.

B. Min-Max Analysis: $CCBR_\tau$ Envelope

In Fig. 6 and Fig. 7, the GPS L1 C/A signal is compared to a Galileo E1B signal at $B_R=24$ MHz. In these figures, the envelope between the minimum and maximum values of the CCBR_τ is displayed. These values can easily be obtained numerically by evaluating the ratio for each value of relative phase. A first interesting remark concerning this display is that the min and max curves occasionally meet at specific path separations, for which the CCBR_τ does not depend on the relative phase. In Fig. 7, one can see that the Galileo signal

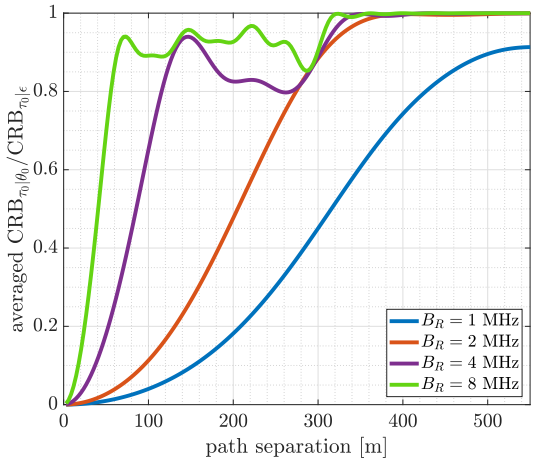

Fig. 5. Averaged CCBR_τ for the GPS L1 C/A PRN 1 signal with B_R = 1, 2, 4, 8 MHz, and ϕ_Γ uniformly distributed in $(0, \pi)$.

might oscillate more within the 300 meters but the CCBR_τ remains above 0.9, while the C/A signal, Fig. 6, presents a depression at around 300m which goes down to 0.75.

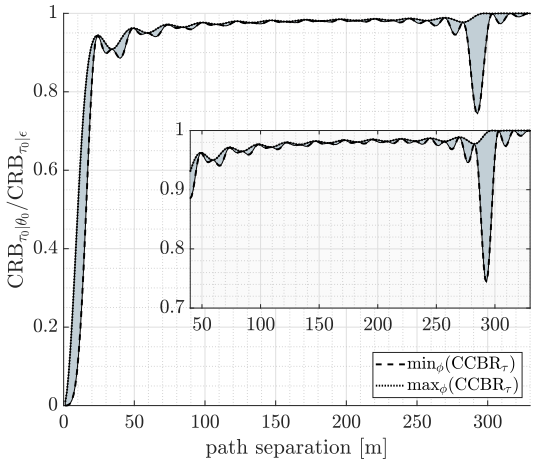

Fig. 6. CCBR_τ envelope for a GPS L1 C/A signal with B_R = 24 MHz.

Fig. 8 and Fig. 9 are two other examples of CCBR_τ envelopes for GPS L5-I and Galileo E5 signals when their entire bandwidth is sampled. These figures focus on the first 50 meters of path separation since the corresponding CCBR_τ are close to 1 for larger path separation. In Fig. 8, the CCBR_τ can vary a lot in the range of path separation between 10 and 20 meters (CCBR_τ is in a 0.4 wide range), then for path separation larger than 30 meters, the multipath does not affect the estimation of the LOS time delay anymore (CCBR_τ larger than 0.9. For the E5 signal, Fig. 9, the shape of the envelope is less smooth, but overall thinner. For a path separation of 10 meters, it presents a large range of possible CCBR_τ values (between 0.6 and 1) but then the CCBR_τ goes above 0.9 at around 20 meters and flattens out. As a conclusive remark for these two figures, the E5 signal is slightly more resilient than the L5 signal when path separation increases since it is almost not affected anymore above 20 meters.

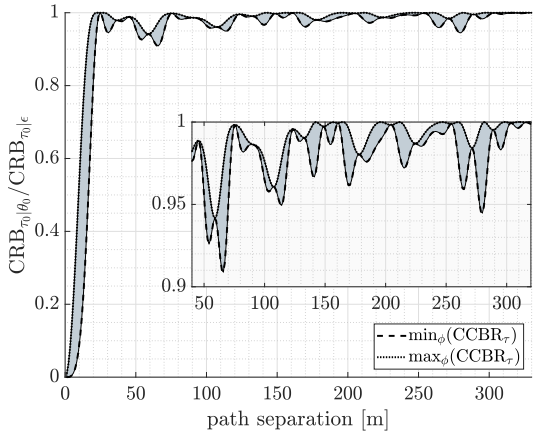

Fig. 7. CCBR_τ envelope for a Galileo E1B signal with B_R = 24 MHz.

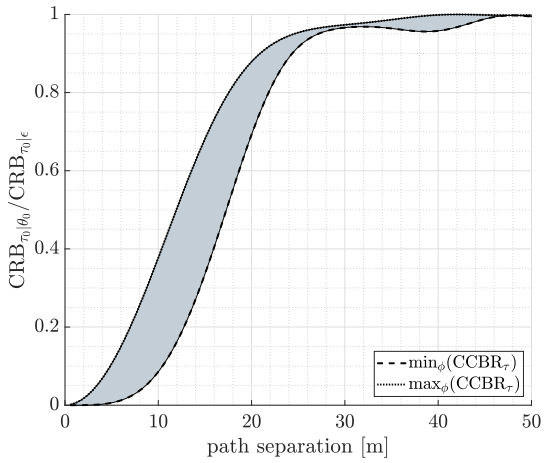

Fig. 8. CCBR_τ envelope for a GPS L5-I signal with B_R = 24 MHz.

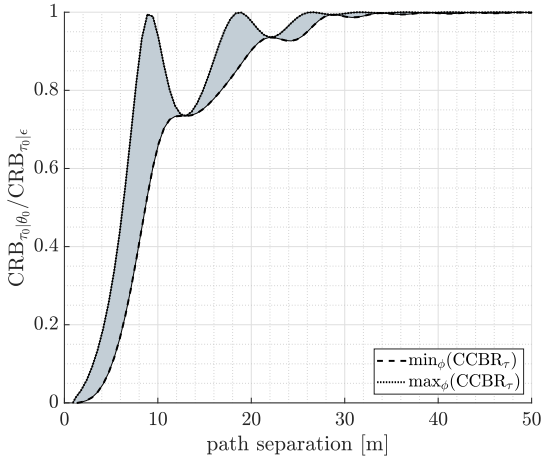

Fig. 9. CCBR_τ envelope for a Galileo E5 signal with B_R = 60 MHz.

C. Performance Considerations

From the results presented in Fig. 6 and Fig. 7, it is then possible to obtain the average RMSE of a given scenario,

assuming a uniformly distributed relative phase ϕ_Γ over $(0, \pi)$. The single source CRB in [26], recalled in (25), is typically shown as a function of the output SNR, defined in (2). Then, for a specific SNR_{out} (i.e., a given receiver operation point), it is simple to use the CCBR_τ to obtain an evaluation of the best achievable accuracy for the time-delay estimation in presence of a single multipath using (27), this is not a bound anymore but it can provide an order of magnitude of the averaged bound:

$$E_{\phi_\Gamma}\left\{\text{CRB}_{\tau_0|\epsilon}\right\} = \frac{\text{CRB}_{\tau_0|\theta_0,\sigma_n^2}}{E_{\phi_\Gamma}\left\{\text{CCBR}_\tau\right\}} \tag{30}$$

Note that the result will consequently be averaged over the possible phase differences.

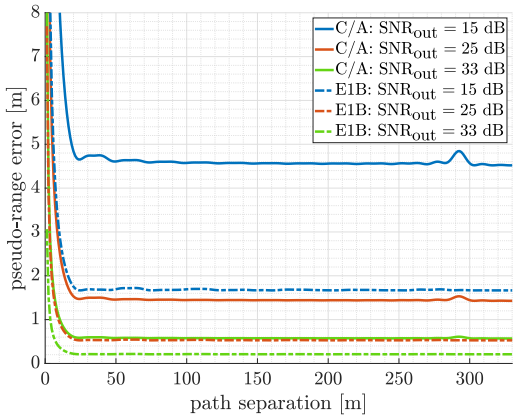

Fig. 10. Averaged $\text{CRB}_{\tau_0|\epsilon}$ in presence of a single multipath as an application of the averaged CCBR_τ on GPS L1 C/A (continuous lines) and Galileo E1B (dashed lines) signals, sampled at B_R = 24 MHz for three different representative SNR_{out}.

Fig. 10 coherently completes the example proposed in [18, Fig. 5], in which the bounds are replaced by a ML-based estimator, and the results are obtained taking the RMSE of several Monte Carlo simulations with random secondary path relative phase. Three representative values of SNR_{out} are considered: SNR_{out} = 15, 25, and 33 dB. Notice that the first value, 15dB, corresponds to a nominal C/N_0 = 45 dB-Hz and T_I = 1ms, the minimum integration time for a GPS L1 C/A signal. The second one, 25dB, under the same nominal conditions, corresponds to a standard integration time T_I = 10ms, and the last one, 33dB, is obtained for instance using an extended integration around 64ms. Equivalently, as done in high-sensitivity receivers, these values may correspond to larger non-coherent integration times for lower C/N_0 values.

It is worth pointing out that the results in Fig. 10 differ from the work presented in [18] when the path separation gets very small (less than 5 meters): where the averaged $\text{CRB}_{\tau_0|\epsilon}$ tends to infinity here, it goes down to a smaller value in [18, Fig. 5]. This is due to the assumptions on the estimator. In [18], the author presents the result of an MMSE estimator considering amplitude of the LOS larger than the NLOS and the LOS signal arriving prior to the NLOS. This estimator appears to be biased. The CRB is a lower bound for any unbiased estimator. If one considers the estimation of two signals very close in time, the CCBR_τ tells that the variance of an unbiased dual source estimator will tend to infinity. This was also pointed out by the same author in [30, Sec. IV], or more recently in [35, Sec. VI].

It is interesting to see how the peak at 300 meter observed in Fig. 6 is reflected: at SNR_{out} = 15 dB, a multipath with a path separation around 300m would then induce an additional 20cm error compared to a slightly different path separation. Such a behavior could be observed in Fig. 3. As expected, the Galileo E1B signal performance is less affected than the C/A signal one, given that the binary offset carrier modulation has a narrower correlation function.

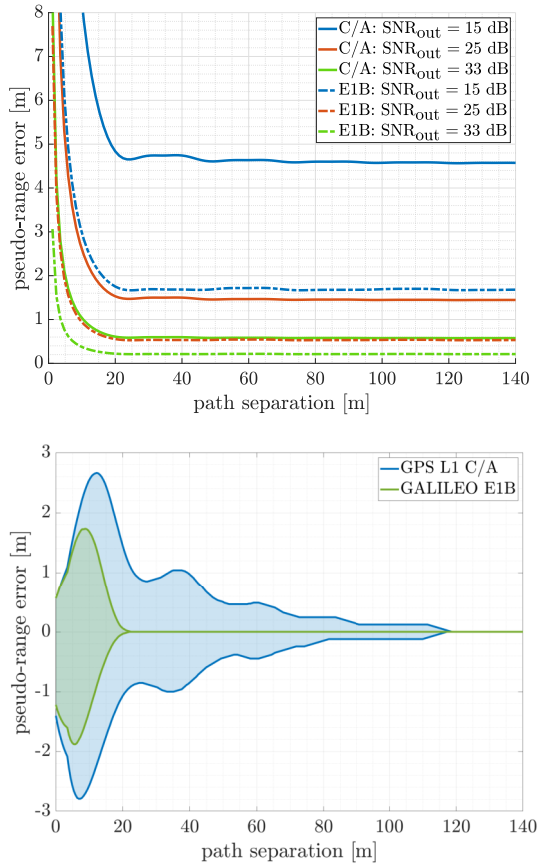

Fig. 11. (**Top**) Averaged $\text{CRB}_{\tau_0|\epsilon}$ in presence of a single multipath as an application of the averaged CCBR_τ on GPS L1 C/A (continuous lines) and Galileo E1B (dashed lines) signals, sampled at B_R = 24 MHz for three different representative SNR_{out}. (**Bottom**) Corresponding MPEE when applying the MEDLL.

Finally, in Fig. 11, the averaged $\text{CRB}_{\tau_0|\epsilon}$ resulting from the CCBR_τ is compared to the information provided by the MPEE in the case of two signals (GPS L1 C/A and GALILEO E1B) when the MEDLL is applied. From these figures, it is possible to see that, due to thermal noise, the best achievable performance of an unbiased estimator may be larger than the actual error predicted by the MPEE. Such a set of figure gives an insight of the contributions of both the error induced by the multipath thanks to the MPEE and the error induced by thermal noise thanks to the CCBR_τ approach. For low SNR_{out} it is clear that the latter is more significant than the former.

D. Regarding the Doppler parameter

In this section, an overview of the potential output of the CCBR_b expressed in (29) is presented. Taking advantage of the π-periodicity of the ratio, an averaged CCBR_b can be obtained by assuming, for instance, a uniform distribution of the relative phases over $(0, \pi)$:

$$E_{\phi_\Gamma}\left\{\mathrm{CCBR}_b\right\}(\Delta\tau, b_0, b_1) = \frac{1}{\pi}\int_0^{\pi} \mathrm{CCBR}_b(\Delta\tau, b_0, b_1, \phi)\mathrm{d}\phi \tag{31}$$

In Fig. 12, the averaged CCBR_b is presented for different receivers' RF front-end. One can remark that when B_R increases, the averaged CCBR_b tends to reach 1 for smaller path separations but oscillations appear for $B_R = 4$ MHz and $B_R = 8$ MHz that lead to make smaller B_R more robust to multipath that larger B_R. As a concrete example, for path separation between 140m and 250m, signals filtered at 2 MHz are less affected by the presence of a multipath for the estimation of the Doppler frequency.

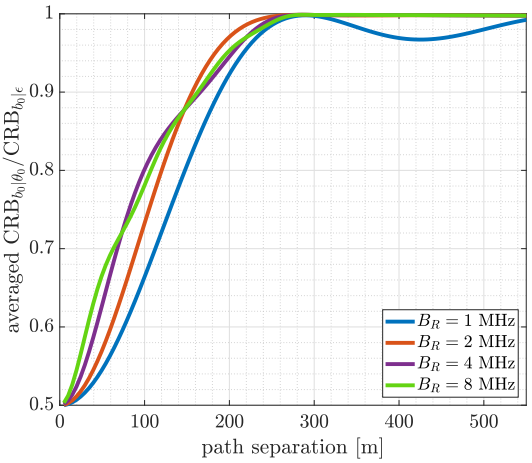

Fig. 12. Averaged CCBR_b for the GPS L1 C/A PRN 1 signal with $B_R = 1, 2, 4, 8$ MHz, and ϕ_Γ uniformly distributed in $(0, \pi)$.

Regarding the min-max approach, Fig. 13 and Fig. 14 present the CCBR_b envelopes for GPS L1 C/A and Galileo E1B. For both figures, it is worth pointing out that there is a relative phase for which the presence of a multipath does not affect the estimation performance of the LOS Doppler frequency. This corresponds to the flat upper bound of the envelopes. Considering GPS L1 C/A signal, the lower bound CCBR_b is smooth and slowly increases up to 1 when the path separation reaches about 300m (or 1 C/A chip). For Galileo E1B signal, the upper bound CCBR_b slope is steeper but oscillates before finally reaching 1 at about 250m of path separation. These observations mean that when the path separation is large enough the LOS Doppler frequency estimation is not affected anymore by the multipath.

E. Cross-Check and Further Investigation

Through the different results provided by the CCBR, there is one that cannot fail to surprise the reader, that is, the remarkable behavior of the GPS L1 C/A CCBR_τ when the path

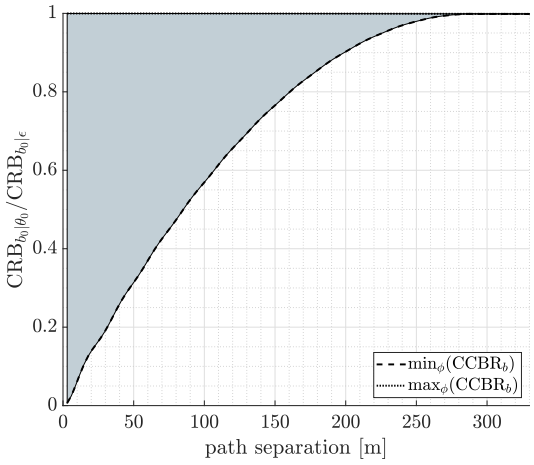

Fig. 13. CCBR_b envelope for a GPS L1 C/A signal with $B_R = 24$ MHz.

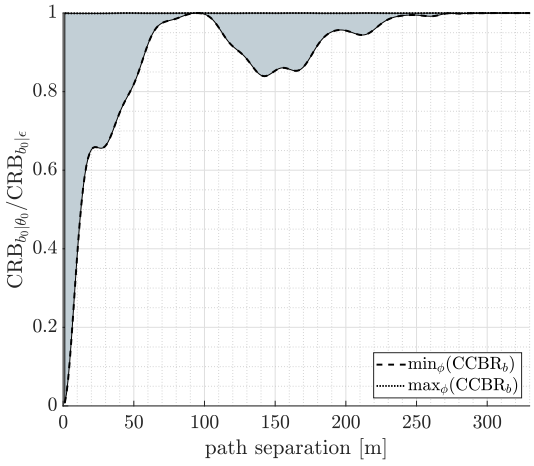

Fig. 14. CCBR_b envelope for a Galileo E1B signal with $B_R = 24$ MHz.

separation is close to 1 C/A chip, or 300m. As a mean to verify this behavior, one can compare the analytical result provided by the CCBR_τ expression with an implementation of the 2S-MLE which is known to turn efficient when the SNR is large enough [31]. Fig. 15, which presents the RMSE of the 2S-MLE for a GPS L1 C/A signal with a RF front-end bandwidth $B_R = 12$ MHz, a multipath in-phase $\Delta\phi = 0$, with MDR= 0.5 and integrated for $T_I = 1$ms, was obtained with 1000 Monte Carlo runs. Here the peak is clearly visible with both analytical and simulation approaches (which are completely independent from one another). Such a methodology has been followed in previous works [26], [27], [36] and leaves no doubt on the exactness of the highlighted behavior.

Finally, since this behavior does not seem to be present for modulations different than BPSK, it is worth looking up at the potential impact of the pseudorandom noise (PRN) sequence used in the GPS simulations. As a matter of fact, it has been recently shown that, for GPS L1 C/A, depending on which PRN is used, the achievable performance can vary significantly [37], [38]. In particular, Gold PRN 7 and 8 are, among others, identified to present the larger difference of

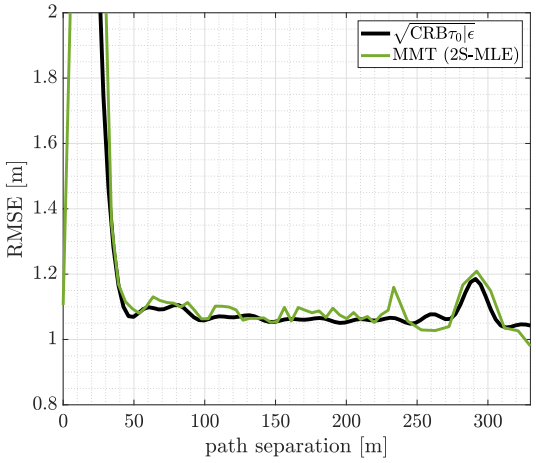

Fig. 15. RMSE of the 2S-MLE (MMT) estimator for GPS L1 C/A signal with corresponding dual source CRB.

performance. Thanks to the easy-to-handle dependency of the CCBR on the baseband signal samples, it is easy to generate the corresponding CCBR_τ for these two PRN codes. In Fig. 16, the averaged CCBR_τ for GPS L1 C/A PRN 7 and 8 are superimposed and the remarkable phenomenon at around 300m is present for both Gold sequences but the amplitude of the depression varies. This extends the fact that the time-delay estimation performance is indeed affected by the Gold sequence choice, even in a dual source context. Moreover, the depression observed at this path separation is present whatever the PRN, which support the idea that it is a consequence of the GPS L1 C/A waveform, namely the BPSK and not a consequence of an unfortunate PRN sequence choice.

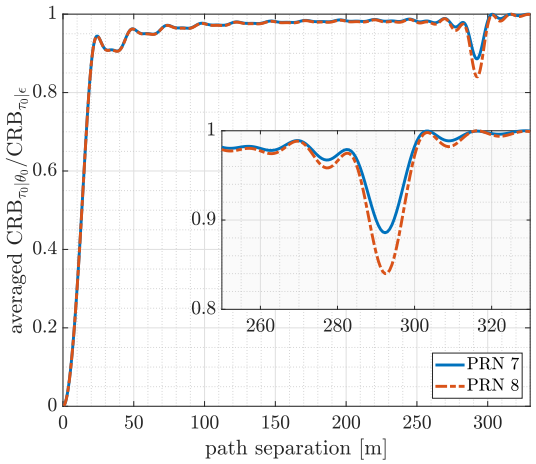

Fig. 16. Averaged CCBR_τ for the GPS L1 C/A signal PRN 7 and 8 with $B_R = 24$ MHz and ϕ_Γ uniformly distributed in $(0, \pi)$.

VI. Conclusion

In this contribution, a criterion for signal robustness to multipath was presented. This criterion, based on a specular multipath model, consists of a ratio between the CRB for the time-delay or Doppler frequency estimation of a signal without multipath and the CRB for the time-delay or Doppler frequency estimation of the same signal distorted by a single multipath. Under the assumption of a unique antenna, both LOS and NLOS signals experience the same thermal noise. As a consequence, this ratio does not depend on the noise level nor the receiver architecture nor, as it is shown in this contribution, the relative amplitude of the reflected path. This simplification and the easy to handle dependency on the relative phase can rapidly lead to quantitative results by fixing the scenario, then avoiding unnecessary restrictive assumptions, the need of a given receiver architecture, or exhaustive evaluations of a given estimator. Using such CRB approach consequently provides information on the best achievable accuracy under multipath conditions in the mean square error sense, which efficiently completes existing criterion, namely the MPEE, that was only providing information on the bias of a given receiver architecture and a given signal. The generality of the proposed CCBR makes it a valuable GNSS signal design and analysis tool. The main features of this metric can be wrapped up as follow:

- it does not depend on any specific receiver architecture: it is valid for any unbiased dual source estimator,
- it takes into account the Doppler effect,
- it is valid for any SNR,
- it does not depend on the relative amplitude of the NLOS signal,
- it is easy to evaluate (closed-form expression),
- it is expressed w.r.t. the signal baseband samples, so it takes into account the potential flaws of the pseudorandom code such as the Gold code ones as it was noticed in [38],
- it provides information on the best achievable accuracy in the mean square error sense.

As a final note, the CCBR can also be used as a powerful complementary tool to study the performance of suboptimal estimators that are asymptotically efficient: the MPEE informs the user when the estimator becomes unbiased and the CCBR provides information on what the corresponding RMSE will look like in this region, given the fact that the noise level is large enough for the estimator to be efficient. The system would then be statistically characterized with its bias and its lower bound variance.

Appendix A

From (16), and omitting the dependency on $\overline{\boldsymbol{\eta}}_2$ for the sake of clarity, the matrix $\boldsymbol{\Phi}$ is defined using the projector $\mathbf{P}_\mathbf{A}$:

$$\boldsymbol{\Phi} = \begin{bmatrix} \frac{\partial \mathbf{a}^H(\eta_0)}{\partial \eta_0} \\ \frac{\partial \mathbf{a}^H(\eta_1)}{\partial \eta_1} \end{bmatrix} \mathbf{P}_\mathbf{A}^\perp \begin{bmatrix} \frac{\partial \mathbf{a}^H(\eta_0)}{\partial \eta_0} \\ \frac{\partial \mathbf{a}^H(\eta_1)}{\partial \eta_1} \end{bmatrix}^H \tag{32}$$

$$= \underbrace{\begin{bmatrix} \frac{\partial \mathbf{a}^H(\eta_0)}{\partial \eta_0} \\ \frac{\partial \mathbf{a}^H(\eta_1)}{\partial \eta_1} \end{bmatrix} \begin{bmatrix} \frac{\partial \mathbf{a}^H(\eta_0)}{\partial \eta_0} \\ \frac{\partial \mathbf{a}^H(\eta_1)}{\partial \eta_1} \end{bmatrix}^H}_{\text{Appendix A-A}}$$

$$\underbrace{-\left[\begin{array}{c}\frac{\partial \mathbf{a}^H(\boldsymbol{\eta}_0)}{\partial \boldsymbol{\eta}_0}\\ \frac{\partial \mathbf{a}^H(\boldsymbol{\eta}_1)}{\partial \boldsymbol{\eta}_1}\end{array}\right]\mathbf{A}\overbrace{\left(\mathbf{A}^H\mathbf{A}\right)^{-1}}^{\text{Appendix A-B}}\mathbf{A}^H\left[\begin{array}{c}\frac{\partial \mathbf{a}^H(\boldsymbol{\eta}_0)}{\partial \boldsymbol{\eta}_0}\\ \frac{\partial \mathbf{a}^H(\boldsymbol{\eta}_1)}{\partial \boldsymbol{\eta}_1}\end{array}\right]^H}_{\text{Appendix A-C}}. \quad (33)$$

A. First Term of (33)

Similarly to the approach in [27], the derivative of $a(t;\boldsymbol{\eta}_i)$ w.r.t. the parameters of interest is

$$\frac{\partial a(t;\boldsymbol{\eta}_i)}{\partial \boldsymbol{\eta}_i} = \mathbf{Q}_i \mathcal{D}(t-\tau_i) e^{-j\omega_c b_i (t-\tau_i)} \quad (34)$$

where

$$\mathbf{Q}_i = \left[\begin{array}{ccc} j\omega_c b_i & 0 & -1 \\ 0 & -j\omega_c & 0 \end{array}\right], \mathcal{D}(t) = \left(\begin{array}{c} s(t) \\ ts(t) \\ s^{(1)}(t) \end{array}\right), \quad (35)$$

with $s^{(1)}(t) = \frac{\mathrm{d}s(t)}{\mathrm{d}t}$. Therefore, when $t = nT_s$, one can write

$$\left[\begin{array}{c}\frac{\partial \mathbf{a}^H(\boldsymbol{\eta}_0)}{\partial \boldsymbol{\eta}_0}\\ \frac{\partial \mathbf{a}^H(\boldsymbol{\eta}_1)}{\partial \boldsymbol{\eta}_1}\end{array}\right] = \mathbf{Q}^* \left[\ldots,\ \overline{\mathcal{D}}(nT_s;\overline{\boldsymbol{\eta}}_2)\mathbf{e}(nT_s;\overline{\boldsymbol{\eta}}_2),\ \ldots\right]^*_{N_1\le n\le N_2} \quad (36)$$

where

$$\mathbf{Q} = \left[\begin{array}{cc} \mathbf{Q}_0 & \mathbf{0} \\ \mathbf{0} & \mathbf{Q}_1 \end{array}\right], \overline{\mathcal{D}}(t;\overline{\boldsymbol{\eta}}_2) = \left[\begin{array}{cc} \mathcal{D}(t-\tau_0) & \mathbf{0} \\ \mathbf{0} & \mathcal{D}(t-\tau_1) \end{array}\right] \quad (37)$$

and $\mathbf{e}(t;\overline{\boldsymbol{\eta}}_2) = \left(\begin{array}{c} e^{-j\omega_c b_0 (t-\tau_0)} \\ e^{-j\omega_c b_1 (t-\tau_1)} \end{array}\right)$. From this result one can write that

$$\begin{aligned}&\left[\begin{array}{c}\frac{\partial \mathbf{a}^H(\boldsymbol{\eta}_0)}{\partial \boldsymbol{\eta}_0}\\ \frac{\partial \mathbf{a}^H(\boldsymbol{\eta}_1)}{\partial \boldsymbol{\eta}_1}\end{array}\right]\left[\begin{array}{c}\frac{\partial \mathbf{a}^H(\boldsymbol{\eta}_0)}{\partial \boldsymbol{\eta}_0}\\ \frac{\partial \mathbf{a}^H(\boldsymbol{\eta}_1)}{\partial \boldsymbol{\eta}_1}\end{array}\right]^H \\ &= \left(\mathbf{Q}\left(\sum_{n=N_1}^{N_2} \overline{\mathcal{D}}(nT_s;\overline{\boldsymbol{\eta}}_2)\left(\mathbf{I}_2 + \boldsymbol{\Delta}_{\boldsymbol{\theta}}(nT_s;\overline{\boldsymbol{\eta}}_2)\right)\overline{\mathcal{D}}(nT_s;\overline{\boldsymbol{\eta}}_2)^H\right)\mathbf{Q}^H\right)^*\end{aligned} \quad (38)$$

with $\boldsymbol{\Delta}_{\boldsymbol{\theta}}$ induced by the difference of delay, Doppler shifts between the two signals,

$$\boldsymbol{\Delta}_{\boldsymbol{\theta}}(nT_s;\overline{\boldsymbol{\eta}}_2) \triangleq \mathbf{e}(nT_s;\overline{\boldsymbol{\eta}}_2)\mathbf{e}(nT_s;\overline{\boldsymbol{\eta}}_2)^H - \mathbf{I}_2. \quad (39)$$

Then, taking the limit of (38) when N_1 and N_2 are very large, it leads to an integral form

$$\begin{aligned}&\lim_{(N_1,N_2)\to(-\infty,+\infty)} \left[\begin{array}{c}\frac{\partial \mathbf{a}^H(\boldsymbol{\eta}_0)}{\partial \boldsymbol{\eta}_0}\\ \frac{\partial \mathbf{a}^H(\boldsymbol{\eta}_1)}{\partial \boldsymbol{\eta}_1}\end{array}\right]\left[\begin{array}{c}\frac{\partial \mathbf{a}^H(\boldsymbol{\eta}_0)}{\partial \boldsymbol{\eta}_0}\\ \frac{\partial \mathbf{a}^H(\boldsymbol{\eta}_1)}{\partial \boldsymbol{\eta}_1}\end{array}\right]^H \\ &= F_s\left(\mathbf{Q}\left[\begin{array}{cc}(\cdot)_{1,1} & (\cdot)_{1,2}\\ (\cdot)_{2,1} & (\cdot)_{2,2}\end{array}\right]\mathbf{Q}^H\right)^*\end{aligned} \quad (40)$$

where $(\cdot)_{1,1} = (\cdot)_{2,2} = \mathbf{W}$ is derived and studied in the single source case in [26], [36] and $(\cdot)_{2,1} = (\cdot)_{1,2}^H = \mathbf{W}^\Delta$ is derived in the dual source case in [27]. For the computation of $\mathbf{W}^\Delta$ no phase difference in the multiplicative complex exponential [27, (14)] is considered since it appears in the $\mathbf{R}_{\boldsymbol{\alpha}}$ matrix defined in (15). Their forms are recalled hereafter,

$$\mathbf{W} = \left[\begin{array}{ccc} w_1 & w_2 & w_3^* \\ w_2 & W_{2,2} & w_4^* \\ w_3 & w_4 & W_{3,3} \end{array}\right], \quad (41)$$

$$\mathbf{W}^\Delta = \left[\begin{array}{ccc} W^\Delta_{1,1} & W^\Delta_{1,2} & W^\Delta_{1,3} \\ W^\Delta_{2,1} & W^\Delta_{2,2} & W^\Delta_{2,3} \\ W^\Delta_{3,1} & W^\Delta_{3,2} & W^\Delta_{3,3} \end{array}\right] e^{j\omega_c b_1 \Delta\tau}, \quad (42)$$

and for the computation of the different terms using the baseband signal samples, the reader may refer to [27].

B. Inverse in the Second Term of (33)

In a similar way, it is possible to evaluate the matrix $\mathbf{A}^H\mathbf{A}$ as follows:

$$\mathbf{A}^H\mathbf{A} = \left[\begin{array}{cc} a(t;\boldsymbol{\eta}_0)^H a(t;\boldsymbol{\eta}_0) & a(t;\boldsymbol{\eta}_0)^H a(t;\boldsymbol{\eta}_1) \\ a(t;\boldsymbol{\eta}_1)^H a(t;\boldsymbol{\eta}_0) & a(t;\boldsymbol{\eta}_1)^H a(t;\boldsymbol{\eta}_1) \end{array}\right], \quad (43)$$

and, when $t = nT_s$ and both N_1 and N_2 are very large, it leads to an integral form:

$$\lim_{(N_1,N_2)\to(-\infty,+\infty)} \mathbf{A}^H\mathbf{A} \quad (44)$$

$$= F_s\left[\begin{array}{cc} w_1 & \left(W^\Delta_{1,1} e^{j\omega_c b_1 \Delta\tau}\right)^* \\ W^\Delta_{1,1} e^{j\omega_c b_1 \Delta\tau} & w_1 \end{array}\right]^*, \quad (45)$$

and then,

$$\begin{aligned}&\lim_{(N_1,N_2)\to(-\infty,+\infty)} \left(\mathbf{A}^H\mathbf{A}\right)^{-1} \\ &= \frac{w_1}{F_s(w_1^2 - |W^\Delta_{1,1}|^2)}\left[\begin{array}{cc} 1 & -\frac{\left(W^\Delta_{1,1} e^{j\omega_c b_1 \Delta\tau}\right)^*}{w_1} \\ -\frac{W^\Delta_{1,1} e^{j\omega_c b_1 \Delta\tau}}{w_1} & 1 \end{array}\right]^*.\end{aligned} \quad (46)$$

C. Second Term of (33)

Again, from (36),one can write that

$$\begin{aligned}\left[\begin{array}{c}\frac{\partial \mathbf{a}^H(\boldsymbol{\eta}_0)}{\partial \boldsymbol{\eta}_0}\\ \frac{\partial \mathbf{a}^H(\boldsymbol{\eta}_1)}{\partial \boldsymbol{\eta}_1}\end{array}\right]\mathbf{A} = \Bigg(\mathbf{Q}\Bigg(\sum_{n=N_1}^{N_2} \overline{\mathcal{D}}(nT_s;\overline{\boldsymbol{\eta}}_2)\left(\mathbf{I}_2 + \boldsymbol{\Delta}_{\boldsymbol{\theta}}(nT_s;\overline{\boldsymbol{\eta}}_2)\right) \\ \times\left[\begin{array}{cc} s(nT_s-\tau_0)^* & 0 \\ 0 & s(nT_s-\tau_1)^* \end{array}\right]\Bigg)\Bigg)^*.\end{aligned} \quad (47)$$

Then, when N_1 and N_2 are very large, it leads to an integral form

$$\lim_{(N_1,N_2)\to(-\infty,+\infty)} \left[\begin{array}{c}\frac{\partial \mathbf{a}^H(\boldsymbol{\eta}_0)}{\partial \boldsymbol{\eta}_0}\\ \frac{\partial \mathbf{a}^H(\boldsymbol{\eta}_1)}{\partial \boldsymbol{\eta}_1}\end{array}\right]\mathbf{A} = F_s\left(\mathbf{Q}\left[\begin{array}{cc} \mathbf{w} & \left(\mathbf{w}^\Delta_{1,.}\right)^H \\ \mathbf{w}^\Delta_{.,1} & \mathbf{w} \end{array}\right]\right)^* \quad (48)$$

where $\mathbf{w}$ is the first column of $\mathbf{W}$ recalled in (41), $\mathbf{w}^\Delta_{.,1}$ is the first column of $\mathbf{W}^\Delta$ recalled in (42) and $\mathbf{w}^\Delta_{1,.}$ is the first row

of $\mathbf{W}^{\Delta}$. Then, combining (48) with (46), the second term of (33) can be written:

$$\begin{aligned}
&\begin{bmatrix} \frac{\partial \mathbf{a}^H(\boldsymbol{\eta}_0)}{\partial \boldsymbol{\eta}_0} \\ \frac{\partial \mathbf{a}^H(\boldsymbol{\eta}_1)}{\partial \boldsymbol{\eta}_1} \end{bmatrix} \mathbf{A}\left(\mathbf{A}^H\mathbf{A}\right)^{-1}\mathbf{A}^H \begin{bmatrix} \frac{\partial \mathbf{a}^H(\boldsymbol{\eta}_0)}{\partial \boldsymbol{\eta}_0} \\ \frac{\partial \mathbf{a}^H(\boldsymbol{\eta}_1)}{\partial \boldsymbol{\eta}_1} \end{bmatrix}^H \\
&\quad = \frac{F_s w_1}{w_1^2 - |W_{1,1}^{\Delta}|^2}\left(\mathbf{Q}\begin{bmatrix} \mathbf{w} & \left(\mathbf{w}_{1,.}^{\Delta}\right)^H \\ \mathbf{w}_{.,1}^{\Delta} & \mathbf{w} \end{bmatrix}\right. \\
&\quad \times \begin{bmatrix} 1 & -\frac{\left(W_{1,1}^{\Delta}\right)^*}{w_1} e^{-j\omega_c b_1 \Delta\tau} \\ -\frac{W_{1,1}^{\Delta}}{w_1} e^{j\omega_c b_1 \Delta\tau} & 1 \end{bmatrix} \\
&\quad \times \left.\begin{bmatrix} \mathbf{w}^H & \left(\mathbf{w}_{.,1}^{\Delta}\right)^H \\ \mathbf{w}_{1,.}^{\Delta} & \mathbf{w}^H \end{bmatrix}\mathbf{Q}^H\right)^* \\
&\quad = \frac{F_s w_1}{w_1^2 - |W_{1,1}^{\Delta}|^2}\left(\mathbf{Q}\begin{bmatrix} (\cdot)_{1,1} & (\cdot)_{1,2} \\ (\cdot)_{2,1} & (\cdot)_{2,2} \end{bmatrix}\mathbf{Q}^H\right)^*
\end{aligned} \tag{49}$$

with

$$\begin{aligned}
(\cdot)_{1,1} &= \mathbf{w}\mathbf{w}^H + \left(\mathbf{w}_{1,.}^{\Delta}\right)^H \mathbf{w}_{1,.}^{\Delta} \\
&\quad - 2\mathrm{Re}\left\{\mathbf{w}\mathbf{w}_{1,.}^{\Delta}\left(\frac{W_{1,1}^{\Delta}}{w_1} e^{j\omega_c b_1 \Delta\tau}\right)^*\right\},
\end{aligned} \tag{50}$$

$$\begin{aligned}
(\cdot)_{2,1} = (\cdot)_{1,2}^H &= \mathbf{w}\mathbf{w}_{1,.}^{\Delta} + \mathbf{w}_{.,1}^{\Delta}\mathbf{w}^H \\
&\quad - \mathbf{w}\mathbf{w}^H \frac{W_{1,1}^{\Delta}}{w_1} e^{j\omega_c b_1 \Delta\tau} - \mathbf{w}_{.,1}^{\Delta}\mathbf{w}_{1,.}^{\Delta}\left(\frac{W_{1,1}^{\Delta}}{w_1} e^{j\omega_c b_1 \Delta\tau}\right)^*,
\end{aligned} \tag{51}$$

$$\begin{aligned}
(\cdot)_{2,2} &= \mathbf{w}\mathbf{w}^H + \mathbf{w}_{.,1}^{\Delta}\left(\mathbf{w}_{.,1}^{\Delta}\right)^H \\
&\quad - 2\mathrm{Re}\left\{\mathbf{w}_{.,1}^{\Delta}\mathbf{w}^H\left(\frac{W_{1,1}^{\Delta}}{w_1} e^{j\omega_c b_1 \Delta\tau}\right)^*\right\}.
\end{aligned} \tag{52}$$

If one subtracts (49) to (38), the matrix $\boldsymbol{\Phi}$ is obtained and $\boldsymbol{\Phi}_{i,j}$ with $i, j = \{1, 2\}$ are the corresponding submatrices when only the terms $(\cdot)_{i,j}$ are used in (38) and (49).

Appendix B

In (17), the real part of the diagonal elements are directly the real part of the $\boldsymbol{\Phi}$ matrix, denoted $\boldsymbol{\Phi}_{1,1}^R$ and $\boldsymbol{\Phi}_{2,2}^R$. On the other hand, the real part of the non-diagonal elements are affected by the complex number Γ:

$$\begin{aligned}
\mathrm{Re}\left\{\Gamma\boldsymbol{\Phi}_{2,1}\right\} &= \mathrm{Re}\left\{\Gamma^*\boldsymbol{\Phi}_{2,1}^H\right\} \\
&= |\Gamma|\left(\cos(\phi_\Gamma)\boldsymbol{\Phi}_{2,1}^R - \sin(\phi_\Gamma)\boldsymbol{\Phi}_{2,1}^I\right).
\end{aligned}$$

where $\boldsymbol{\Phi}_{2,1}^R$ and $\boldsymbol{\Phi}_{2,1}^I$ are the real and imaginary parts of $\boldsymbol{\Phi}_{2,1}$, respectively. Then, in order to obtain a closed-form of $\mathbf{CRB}_{\boldsymbol{\eta}_0|\boldsymbol{\epsilon}}(\boldsymbol{\epsilon})$, the block matrix inversion lemma is used:

$$\begin{bmatrix} \mathbf{A}_{1,1} & \mathbf{A}_{1,2} \\ \mathbf{A}_{2,1} & \mathbf{A}_{2,2} \end{bmatrix}^{-1} = \begin{bmatrix} \mathbf{C}_1^{-1} & -\mathbf{A}_{1,1}^{-1}\mathbf{A}_{1,2}\mathbf{C}_2^{-1} \\ -\mathbf{C}_2^{-1}\mathbf{A}_{2,1}\mathbf{A}_{1,1}^{-1} & \mathbf{C}_2^{-1} \end{bmatrix}$$

$$\mathbf{C}_1 = \mathbf{A}_{1,1} - \mathbf{A}_{1,2}\mathbf{A}_{2,2}^{-1}\mathbf{A}_{2,1}, \tag{53}$$

$$\mathbf{C}_2 = \mathbf{A}_{2,2} - \mathbf{A}_{2,1}\mathbf{A}_{1,1}^{-1}\mathbf{A}_{1,2}, \tag{54}$$

From (53),

$$\begin{aligned}
\mathbf{CRB}_{\boldsymbol{\eta}_0|\boldsymbol{\epsilon}}^{-1}(\boldsymbol{\epsilon}) &= \frac{2\rho_0^2}{\sigma_n^2}\left(\boldsymbol{\Phi}_{1,1}^R - |\Gamma|\left(\cos(\phi_\Gamma)\boldsymbol{\Phi}_{2,1}^R - \sin(\phi_\Gamma)\boldsymbol{\Phi}_{2,1}^I\right)\right. \\
&\quad \times \left.\frac{1}{|\Gamma|^2}\left(\boldsymbol{\Phi}_{2,2}^R\right)^{-1}|\Gamma|\left(\cos(\phi_\Gamma)\boldsymbol{\Phi}_{2,1}^R - \sin(\phi_\Gamma)\boldsymbol{\Phi}_{2,1}^I\right)\right) \\
&= \frac{2\rho_0^2}{\sigma_n^2}\left(\boldsymbol{\Phi}_{1,1}^R - \left(\cos(\phi_\Gamma)\boldsymbol{\Phi}_{2,1}^R - \sin(\phi_\Gamma)\boldsymbol{\Phi}_{2,1}^I\right)\right. \\
&\quad \times \left.\left(\boldsymbol{\Phi}_{2,2}^R\right)^{-1}\left(\cos(\phi_\Gamma)\boldsymbol{\Phi}_{2,1}^R - \sin(\phi_\Gamma)\boldsymbol{\Phi}_{2,1}^I\right)\right).
\end{aligned}$$

Then, simply developing the expression and rearranging the matrices in terms of $\cos(2\phi_\Gamma)$ and $\sin(2\phi_\Gamma)$, the wanted expression (18) is obtained.

References

[1] P. J. G. Teunissen and O. Montenbruck, Eds., *Handbook of Global Navigation Satellite Systems*. Switzerland: Springer, 2017.

[2] C. Fernández-Prades, L. Lo Presti, and E. Falletti, "Satellite Radiolocalization from GPS to GNSS and Beyond: Novel Technologies and Applications for Civil Mass Market," *Proc. of the IEEE*, vol. 99, no. 11, pp. 1882–1904, Nov. 2011.

[3] V. U. Zavorotny, S. Gleason, E. Cardellach, and A. Camps, "Tutorial on Remote Sensing Using GNSS Bistatic Radar of Opportunity," *IEEE Geosci. Remote Sens. Mag.*, vol. 2, no. 4, pp. 8–45, Dec. 2014.

[4] V. U. Zavorotny, K. M. Larson, J. J. Braun, E. E. Small, E. D. Gutmann, and A. L. Bilich, "A Physical Model for GPS Multipath Caused by Land Reflections: Toward Bare Soil Moisture Retrievals," *IEEE Journal of Selected Topics in Applied Earth Observations and Remote Sensing*, vol. 3, no. 1, pp. 100–110, 2010.

[5] L. Lestarquit, M. Peyrezabes, J. Darrozes, E. Motte, N. Roussel, G. Wautelet, F. Frappart, G. Ramillien, R. Biancale, and M. Zribi, "Reflectometry With an Open-Source Software GNSS Receiver: Use Case With Carrier Phase Altimetry," *IEEE Journal of Selected Topics in Applied Earth Observations and Remote Sensing*, vol. 9, no. 10, pp. 4843–4853, 2016.

[6] F. Martin *et al.*, "Mitigation of Direct Signal Cross-Talk and Study of the Coherent Component in GNSS-R," *IEEE Geosci. Remote. Sens. Lett.*, vol. 12, no. 2, pp. 279–283, Feb. 2015.

[7] C. Lubeigt, L. Ortega, J. Vilà-Valls, L. Lestarquit, and E. Chaumette, "On the Impact and Mitigation of Signal Crosstalk in Ground-Based and Low Altitude Airborne GNSS-R," *Remote Sensing*, vol. 13, no. 6, p. 1085, 2021.

[8] M. Paonni and M. Bavaro, "On the Design of a GNSS Acquisition Aiding Signal," in *Proceedings of the 26th International Technical Meeting of The Satellite Division of the Institute of Navigation (ION GNSS+), Nashville, TN*, 2013, pp. 1445–1456.

[9] X. Liu, M. Liang, Y. Morton, P. Closas, T. Zhang, and ZhigangHong, "Performance Evaluation of MSK and OFDM Modulations for Future GNSS Signals," *GPS Solutions*, vol. 18, no. 4, Feb. 2014.

[10] R. Xue, Y. Sun, and D. Zhao, "CPM Signals for Satellite Navigation in the S and C Bands," *Sensors*, vol. 15, pp. 13 184–13 200, June 2015.

[11] L. Ortega, C. Poulliat, M.-L. Boucheret, M. Aubault, and H. A. Bitar, "New Solutions on the Design of a Galileo Acquisition-Aiding Signal to Improve the TTFF and the Sensitivity," in *Proc. ION ITM*, 2018.

[12] E. Kaplan and C. Hegarty, *Understanding GPS/GNSS: Principle and Applications*, 3rd ed. Artech House, 2017.

[13] Y. J. Morton, F. Van Diggelen, J. J. Spilker Jr, B. W. Parkinson, and S. L. G. Gao, *Position, Navigation, and Timing Technologies in the 21st Century, Volumes 1 and 2*. John Wiley & Sons, 2020.

[14] P. J. G. Teunissen and O. Montenbruck, Eds., *Handbook of Global Navigation Satellite Systems*. Switzerland: Springer, 2017.

[15] J. Jones, P. Fenton, and B. Smith, "Theory and Performance of the Pulse Aperture Correlator," NovAtel Inc., Tech. Rep., 2004. [Online]. Available: https://hexagondownloads.blob.core.windows.net/public/Novatel/assets/Documents/Papers/PAC/PAC.pdf

[16] P. C. Fenton and J. Jones, "The Theory and Performance of NovAtel Inc.'s Vision Correlator," *Proceedings of the 18th International Technical Meeting of the Satellite Division of The Institute of Navigation*, pp. 2178–2186, January 2005.

[17] G. A. McGraw and M. S. Braasch, "GNSS multipath Mitigation using Gated and High Resolution Correlator Concepts," in *Proceedings of the 1999 National Technical Meeting of The Institute of Navigation*, 1999, pp. 333–342.

[18] L. R. Weill, "Multipath Mitigation using Modernized GPS Signals: How Good Can it Get?" *Proceedings of the 15th International Technical Meeting of the Satellite Division of The Institute of Navigation (ION GPS 2002)*, pp. 493–505, September 2002.

[19] R. D. Van Nee, "The Multipath Estimating Delay Lock Loop," in *IEEE Second International Symposium on Spread Spectrum Techniques and Applications*, 1992, pp. 39–42.

[20] B. R. Townsend, P. C. Fenton, K. J. Van Dierendonck, and R. D. J. Van Nee, "Performance Evaluation of the Multipath Estimating Delay Lock Loop," *Navigation*, vol. 42, no. 3, pp. 502–514, 1995. [Online]. Available: https://onlinelibrary.wiley.com/doi/abs/10.1002/j.2161-4296.1995.tb01903.x

[21] B. H. Fleury, M. Tschudin, R. Heddergott, D. Dahlhaus, and K. Ingeman Pedersen, "Channel parameter estimation in mobile radio environments using the SAGE algorithm," *IEEE Journal on Selected Areas in Communications*, vol. 17, no. 3, pp. 434–450, 1999.

[22] X. Chen, F. Dovis, M. Pini, and P. Mulassano, "Turbo Architecture for Multipath Mitigation in Global Navigation Satellite System Receivers," *IET Radar, Sonar & Navigation*, vol. 5, no. 5, pp. 517–527, 2011.

[23] X. Chen and F. Dovis, "Enhanced CADLL Structure for Multipath Mitigation in Urban Scenarios," in *Proceedings of the 2011 International Technical Meeting of The Institute of Navigation*, 2011, pp. 678–686.

[24] A. Jovanovic, Y. Tawk, C. Botteron, and P.-A. Farine, "Multipath Mitigation Techniques for CBOC, TMBOC and AltBOC Signals using Advanced Correlators Architectures," in *IEEE/ION Position, Location and Navigation Symposium*, 2010, pp. 1127–1136.

[25] X. Chen, F. Dovis, S. Peng, and Y. Morton, "Comparative Studies of GPS Multipath Mitigation Methods Performance," *IEEE Transactions on Aerospace and Electronic Systems*, vol. 49, no. 3, pp. 1555–1568, 2013.

[26] D. Medina, L. Ortega, J. Vilà-Valls, P. Closas, F. Vincent, and E. Chaumette, "A New Compact CRB for Delay, Doppler and Phase Estimation - Application to GNSS SPP & RTK Performance Characterization," *IET Radar, Sonar & Navigation*, Jun 2020.

[27] C. Lubeigt, L. Ortega, J. Vilà-Valls, L. Lestarquit, and E. Chaumette, "Joint Delay-Doppler Estimation Performance in a Dual Source Context," *Remote Sensing*, vol. 12, no. 23, 2020. [Online]. Available: https://www.mdpi.com/2072-4292/12/23/3894

[28] C. Hegarty, M. Tran, and J. W. Betz, "Multipath Performance of the New GNSS Signals," in *Proceedings of the 2004 National Technical Meeting of The Institute of Navigation*, 2004, pp. 333–342.

[29] N. Blanco-Delgado and F. D. Nunes, "Multipath Estimation in Multicorrelator GNSS Receivers using the Maximum Likelihood Principle," *IEEE Trans. Aerosp. Electron. Syst.*, vol. 48, no. 4, pp. 3222–3233, Oct. 2012.

[30] L. R. Weill, "Achieving Theoretical Accuracy Limits for Pseudoranging in the Presence of Multipath," in *Proceedings of the 8th International Technical Meeting of the Satellite Division of the Institute of Navigation (ION GPS 1995)*, 1995, pp. 1521–1530.

[31] A. Renaux, P. Forster, E. Chaumette, and P. Larzabal, "On the High-SNR Conditional Maximum-Likelihood Estimator Full Statistical Characterization," *IEEE Trans. Signal Process.*, vol. 54, no. 12, pp. 4840 – 4843, Dec. 2006.

[32] H. L. Van Trees, *Part III: Radar-Sonar Signal Processing and Gaussian Signals in Noise*, ser. Detection, Estimation, and Modulation Theory. Wiley, 2001.

[33] H. L. Van Trees, *Part I: Detection Estimation and Linear Modulation Theory*, ser. Detection, Estimation, and Modulation Theory. Wiley, 2001.

[34] B. Ottersten, M. Viberg, P. Stoica, and A. Nehorai, "Exact and Large Sample Maximum Likelihood Techniques for Parameter Estimation and Detection in Array Processing," in *Radar Array Processing*, S. Haykin, J. Litva, and T. J. Shepherd, Eds. Heidelberg: Springer-Verlag, 1993, ch. 4, pp. 99–151.

[35] M. Sahmoudi and M. M. G. Amin, "Fast Iterative Maximum-Likelihood Algorithm (FIMLA) for Multipath Mitigation in the Next Generation of GNSS Receivers," *IEEE Transactions on Wireless Communications*, vol. 7, no. 11, pp. 4362–4374, 2008.

[36] P. Das, J. Vilà-Valls, F. Vincent, L. Davain, and E. Chaumette, "A New Compact Delay, Doppler Stretch and Phase Estimation CRB with a Band-Limited Signal for Generic Remote Sensing Applications," *Remote Sensing*, vol. 12, no. 18, p. 2913, 2020.

[37] W. Li, E. Cardellach, F. Fabra, S. Ribó, and A. Rius, "Effects of PRN-Dependent ACF Deviations on GNSS-R Wind Speed Retrieval," *IEEE Geosci. Remote Sens. Lett.*, vol. 16, no. 3, pp. 327–331, March 2018.

[38] L. Ortega, J. Vilà-Valls, E. Chaumette, and F. Vincent, "On the Time-Delay Estimation Performance Limit of New GNSS Acquisition Codes," in *ICL-GNSS 2020*. IEEE, 2020, pp. 1–6.

Corentin Lubeigt is at the Télécommunications pour le Spatial et l'Aéronautique laboratory (TéSA) and the Institut Supérieur de l'Aéronautique et de l'Espace (ISAE-SUPAERO), University of Toulouse, France. He received the MS in Engineering at ISAE-SUPAERO in 2018 and is currently preparing a PhD in signal processing for GNSS-R.

Lorenzo Ortega is Associate Profesor at Institut Polytechnique des Sciences Avancées (IPSA), Toulouse, France. He received the MS in Electrical Engineering from Zaragoza University, Spain, in 2016 and PhD in Signal Processing from National Polytechnic Institute of Toulouse (INPT) in 2019. From 2020 to 2021, he was a postdoctoral researcher at the Institut Supérieur de l'Aéronautique et de l'Espace (ISAE-SUPAERO), University of Toulouse, France. His primary areas of interest include statistical signal processing, machine learning, estimation and detection theory, channel coding and digital communications, with applications to satellite communication, localization, tracking, navigation and remote sensing.

Jordi Vilà-Valls (S'08 – M'13 – SM'17) is Associate Professor at the Institut Supérieur de l'Aéronautique et de l'Espace (ISAE-SUPAERO), University of Toulouse, France. He received the MS in Electrical Engineering from both Universitat Politècnica de Catalunya (UPC), Spain, and Grenoble Institute of Technology (INPG), France, in 2006, and the PhD in Signal Processing from INPG in 2010. His primary areas of interest include statistical signal processing, estimation and detection theory, nonlinear Bayesian inference and robust filtering, with applications to localization, tracking, navigation and remote sensing. He is Elected Member of the EURASIP TAC on Theoretical and Methodological Trends in Signal Processing, AE for Signal Processing, and has been (is) actively involved in the organizing committees of EUSIPCO (2019, 2021, 2024) and IEEE CAMSAP (2019, 2023).

Laurent Lestarquit is a GNSS signal expert, at the French space agency (CNES) in Toulouse. He is currently involved in research in the field of GNSS scientific use for earth and atmosphere remote sensing and GNSS signal metrology. He graduated from the Ecole Polytechnique, Paris, France, in 1994 and received his space engineering diploma from Supaero (now ISAE) in 1996. He received the 2017 European Inventor Award from the European Patent Office for the invention of the Alt-BOC modulation and the CBOC waveform now used in GALILEO.

Eric Chaumette was born in 1965 at Chartres (France). He studied Electronics and Signal Processing both at ENAC (Toulouse, France) where he obtained an Engineer degree in 1989, and at Toulouse University where he obtained a M.Sc. degree in Signal Processing in 1989. From 1990 to 2007, he was with Thales in various radar studies departments. From 2007 to 2013, he was with the Electromagnetic and Radar Division of the French Aerospace Lab (ONERA), Palaiseau, France, as a research engineer. Simultaneously, from 2000 to 2014, he was a research associate at laboratory SATIE, CNRS, École Normale Supérieure de Cachan, France, where he received the PhD degree in 2004 and the "habilitation à diriger les recherches" in 2014. He is currently Professor at the Department of Electronics, Optronics and Signal of ISAE-SUPAERO, Toulouse, France. Main domains of interest are related to detection and estimation theory applied to localisation and navigation (GNSS, robust multi-sensor data fusion).